ETH
Eidgenössische Technische Hochschule Zürich
Swiss Federal Institute of Technology Zurich

D PHYS

Niklas Viebig
20-944-286

Analysis of a Grating Nuller for LIFE

Semester Thesis

Master's Degree Programme in Physics
Exoplanet and Habitability Group
Swiss Federal Institute of Technology (ETH) Zurich

Supervision

Prof. Dr. Sascha Patrick Quanz

Thomas Birbacher

March, 2025

Abstract

The Large Interferometer For Exoplanets (LIFE) aims to utilize advanced nulling techniques to enhance direct imaging capabilities of exoplanets. One potential candidate for such a system is a grating nuller, a device that exploits diffraction to achieve destructive interference.

This report investigates the applicability of a grating nuller for nulling interferometry. We derive the nulling condition and the expected throughput for a sinusoidal phase grating and provide a theoretical framework to assess its performance. We further propose an experimental setup to validate these findings. Under ideal conditions, we find that a grating nuller achieves a theoretical throughput of approximately 25% for the proposed setup.

Our results highlight both the strengths and limitations of the grating nuller as a potential component for LIFE. The key advantages include its intrinsic achromaticity and geometric simplicity which could make it an attractive alternative to conventional interferometric designs. However, an expected low throughput presents a significant challenge. Given these constraints, while a grating nuller could contribute to nulling interferometry, its practical feasibility for LIFE remains unlikely and experimental testing is necessary for a conclusive result.

Contents

Chapter 1

Introduction

The hunt for exoplanets has been a major focus in astrophysics since the mid-1990s. The scientific goal of these observations is to characterize the atmospheres of exoplanets and to understand the origin and development of life. Answering these questions will help us understand life on earth and how to preserve it. With advancements in technology and the development of a new generation of ground- and space-based telescopes, such as the James Webb Space Telescope, over 5,600 [1] exoplanets have now been detected and classified. But apart from perhaps the HWO, so far no mission has been put together with the sole aim of imaging exoplanets. To achieve this we need a more advanced array of telescopes.

The LIFE (Large Interferometer For Exoplanets) initiative is a space-based mission proposed by the Exoplanet and Habitability Group at ETH Zurich, aimed at searching for life beyond our solar system and investigating the possibility of life on exoplanets [2]. What distinguishes the LIFE mission from other telescopes, such as the Extremely Large Telescope (ELT) in Chile or the proposed Habitable Worlds Observatory (HWO), is its focus on observing the mid-infrared (MIR) spectrum. While the ELT and HWO are designed to observe ultraviolet (UV) to near-infrared (NIR) wavelengths, the LIFE missions emphasis on the MIR offers several advantages [3][4] :

- Atmospheric abundances retrieved from thermal emission spectra offer accuracy and precision comparable to those from reflected light observations.

- Biosignature gases like CH_4 and N_2O, along with the anti-biosignature gas CO, are detectable exclusively in thermal emission spectra.

- Although O_2 is only observable in reflected light, its by-product O_3, visible in the MIR thermal emission spectrum, serves as a reliable proxy for oxygen.

- Planetary radius constraints are significantly tighter in thermal emission, with uncertainties around 5%, compared to the 30% uncertainties in reflected light.

- Surface temperature and pressure can be accurately determined from thermal emission data, whereas reflected light provides limited information on temperature and weaker constraints on pressure.

One of the big challenges in detecting exoplanets is that they are far dimmer than the stars they orbit. In the visible spectrum, stars are typically more luminous than planets by a factor of around 10^{10}. In contrast, in the infrared spectrum, the difference between the brightness of stars and planets is smaller, with a typical luminosity ratio of around 10^6 to 10^5. This is because planets emit thermal radiation in the infrared, especially those that are cooler or larger [5].

Even in the mid-infrared, the star's brightness still poses a significant problem. To overcome this, several techniques have been developed to suppress the stars light and enhance the planets visibility. One of these methods is nulling interferometry. Nulling interferometry is a technique used in astronomy to help detect faint objects, like exoplanets, that are close to bright object like stars. The idea is to destructively interfere the light of the star so that only the weak light of the planet remains.

Figure 1.1a shows the simplest setup for such a nulling interferometer, a Bracewell interferomter[8]. The light from the star and from the planet enter the two telescopes. These beams are recombined with a phase shift of π introduced to one of the beams. This phase shift causes destructive interference for the starlight, as it is approximately coherent and originates from a single point source. The planetary light does not destructively interfere due to differing path lengths from the angle of incidence. This results in a detectable signal. Figure 1.1 shows the resulting fringe pattern of such an observation. The star is positioned in the central dark fringe while the planets are radial distributed around the star. By rotating the setup around the position of the star the whole sky can be mapped and planets around the star can be found. This leads to the transmission spectra dependent on the rotational angle, as demonstrated in the Figure.

The LIFE mission has implemented an X-array architecture. It consists of four collector spacecraft arranged in a 6:1 rectangular configuration, with a central combiner spacecraft positioned at the geometric center. The shorter separation between collectors, denoted b, is referred to as the null baseline, while the longer separation,

(a) Two element nulling interferometer. [6]

(b) Transmission map explaining nulling of starlight (black and white fringes) while preserving planetary signals. Rotating the telescope along the line of sight leads to the different transmission spectra of the three planets with varying distance to the star. [7]
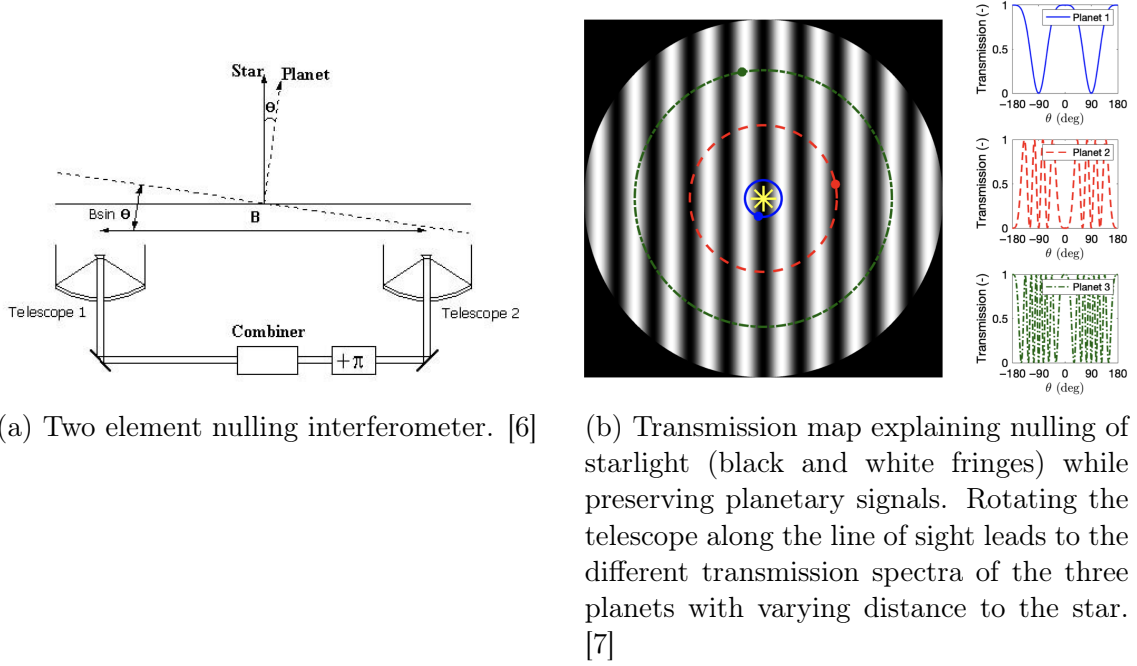
Figure 1.1: Workings of a grating nuller, figure adapted from [5]

qb, represents the imaging baseline. The interferometer consists of two chopped Bracewell beam combiners. [9]

The goal of this report is to provide a theoretical understanding of the workings of a grating nuller. In Chapter 2, we analyze the theoretical principles of a grating nuller using the mathematical framework of Fourier Optics, first considering the case of monochromatic light before extending the discussion to achromatic behavior. Chapter 3 introduces a proposed experimental setup and evaluates its expected performance based on the theoretical model. Unfortunately, due to unforeseen delivery delays of essential components, we were unable to construct and test the setup experimentally. Therefore, this report focuses on developing a theoretical foundation and providing a detailed analysis of the intended experimental design, which can serve as groundwork for future experimental verification. The code related to this analysis is available on GitHub.

Chapter 2

Theory of grating nullers

The LIFE mission aims to measure across a wavelength range from 4 to 18.5 micrometers [10]. One approach to measure along such a broad range of wavelengths is the use of a grating nuller, first proposed by Stefan Martin [11]. Unlike other nulling interferometers, such as configuration currently used in NICE, the grating nuller offers a key advantage: it requires fewer optical components and maintains fewer separate beam paths, making it easier to align and control. A particularly attractive property of the grating nuller is its intrinsic achromaticity, meaning it can maintain destructive interference (nulling) over a broad range of wavelengths.

A basic layout for such a grating nuller is shown in Figure 2.1. Starlight enters the aperture from the left, strikes an amplitude mask that splits the beam into two. These two beams are then collimated onto a phase grating, where each beam is diffracted into several diffraction orders. According to the grating equation

$$m\lambda = d\left(\sin\theta_{\text{incident}} + \sin\theta_{\text{diffracted}}\right) \tag{2.1}$$

where m is the diffraction order, λ is the wavelength, d is the grating spacing, and θ_{incident} and $\theta_{\text{diffracted}}$ are the angles of the incident and diffracted light, the output angle of the m-th order depends on the input angle of the beam. This means that
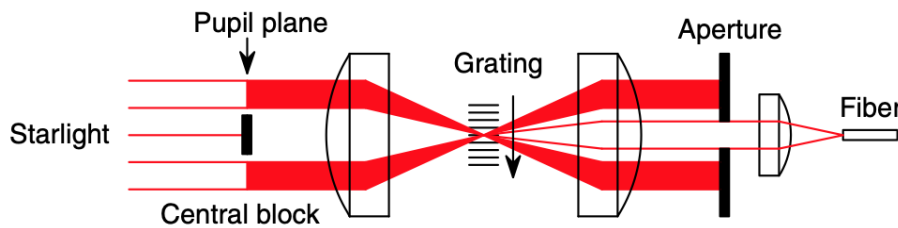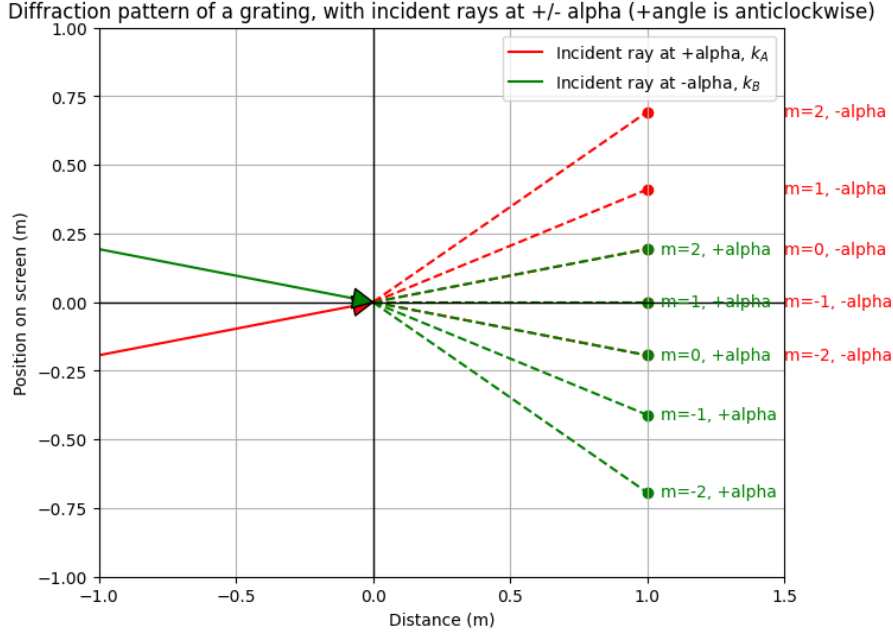

Figure 2.1: A basic layout for a grating nuller [11].

Figure 2.2: This figure illustrates the diffraction pattern of a grating when two incident beams enter at angles $\pm\alpha$. The initial rays (solid lines) are diffracted into multiple orders (dashed lines) according to the grating equation. The positions of the diffracted orders on the screen depend on the wavelength and grating spacing. The green and red rays represent diffraction from the two incident beams, highlighting the symmetry of the diffraction process

if we choose the angle such that the +1 order of the upper beam and the -1 order of the lower beam both have an output angle of 0, they will interfere, as depicted in the figure 2.2.

Interesting is, that the kind of interference, constructively or destructively can now be influenced by the relative position of the grating. To explain this effect and why the setup is intrinsically achromatic we begin by observing two beams at a single wavelength.

2.1   Single wavelength case

For simplicity we consider two plane waves, $U_A(\vec{r})$ and $U_B(\vec{r})$, propagating at angles θ_A and θ_B relative to the z-axis in the y = 0 plane. Each wave is described by:

$$U_i(\vec{r}, t) = U_0 e^{i(\vec{k}_i \cdot \vec{r} - \omega t)}, \tag{2.2}$$

$i \in \{A, B\}$, where U_0 is the amplitude, $\vec{k}_A$ and $\vec{k}_B$ are the wave vectors for waves A and B, respectively, and ω is the angular frequency. The wave vectors $\vec{k}_A$ and $\vec{k}_B$

can be expressed as:

$$\vec{k}_A = k \begin{pmatrix} \sin(\theta) \\ 0 \\ \cos(\theta) \end{pmatrix}, \quad \vec{k}_B = k \begin{pmatrix} -\sin(\theta) \\ 0 \\ \cos(\theta) \end{pmatrix}. \tag{2.3}$$

where $k = \frac{2\pi}{\lambda}$ is the wave-number and λ is the wavelength. The total field U_{tot} at the surface of the grating is the superposition of U_A and U_B.

The grating lies in the $z = 0$ plane. The effect of a grating on an incoming beam can be described by Fourier Optics [12]. In that formalism, the impact of the grating is described by multiplying the transfer function of the grating with the beam at the plane of entry, which in our case is the $z = 0$ plane. This results in the modified electric field $U'(x, y, z = 0)$, which describes the field immediately after the grating:

$$U'(x, y, z = 0) = t(x)U(x, y, z = 0), \tag{2.4}$$

where $t(x)$ is the transmission function of the grating.

Mathematically, we describe a phase grating as a structure with a periodic phase modulation in one direction. The general transmission function of a phase grating, denoted as $t(x)$, can be expressed as:

$$t(x) = \exp\left[i\phi(x)\right],$$

where $\phi(x)$ represents the phase modulation introduced by the grating. This modulation is periodic with a period Λ, meaning:

$$\phi(x + \Lambda) = \phi(x).$$

Since diffraction occurs when a wavefront encounters a periodic structure, the phase modulation function $\phi(x)$ determines how the incident light is redistributed among different diffraction orders. The intensity of each diffraction order is given by the Fourier coefficients of $\phi(x)$, highlighting the role of Fourier optics in analyzing and designing phase gratings. The transmission function describes how the phase grating diffracts incident light into multiple orders, with the intensity of each diffraction order determined by the Fourier coefficients of the periodic phase function $\phi(x)$.

In this report, we will discuss further a sinusoidal phase grating, for which $\phi(x)$

can be expressed as:

$$\phi(x) = \phi_0 \sin\left(\frac{2\pi x}{\Lambda}\right)$$

where ϕ_0 is the modulation of the peak phase.

To analyze the effect of this grating on an incident field $U(x, y, z = 0)$, we decompose the transmission function $t(x)$ into its Fourier series expansion using the Jacobi-Anger identity [13]:

$$t(x) = \sum_{m=-\infty}^{\infty} J_m(\phi_0) e^{i\frac{2\pi m x}{\Lambda}}, \tag{2.5}$$

where $J_m(\phi_0)$ are the Bessel functions of the first kind of order m.

To then calculate the field at a position $z = d$ away from the grating, we again use the Fourier Optics formalism. The propagation of the field can be expressed as a convolution of the modified field $U'(x, y, z = 0)$ with the free-space propagation function $h(x, y, z = d)$. The resulting field at $z = d$ is given by:

$$U(x, y, z = d) = \iint_{-\infty}^{\infty} U'(x', y', z = 0)\, h(x - x', y - y', z = d) dx' dy', \tag{2.6}$$

where the free-space propagation function $h(x, y, z)$ is given by:

$$h(x, y, z) = \frac{e^{ikz}}{i\lambda z} e^{\frac{ik}{2z}(x^2+y^2)} \tag{2.7}$$

By substituting $U'(x', y', z = 0) = t(x')U(x', y', z = 0)$ into the integral, the full expression becomes:

$$U(x, y, z = d) = \iint_{-\infty}^{\infty} t(x')U(x', y', z = 0)\, h(x - x', y - y', z = d) dx' dy' \tag{2.8}$$

We are only interested in $U(x = 0, y = 0, z)$, as this is along where our constructed beam propagates. We can use Eq. 2.8 to derive an expression for the field. To calculate how much we need to displace the grating to create destructive interference between the two beams, we introduce the displacement value a_{min} so that the field after the grating becomes

$$U'(x, y, z = 0) = t(x)U(x, y, z = 0) = t(x)(U_A(x + a) + U_B(x + a)).$$

We can solve the integral in eqs 2.8 as presented in appendix 6.1. This results in a electric field

$$
\begin{aligned}
U(0,0,z) = U_0 h_0 \Bigg[& e^{ik\sin(\theta)a} \sum_{q=-\infty}^{\infty} \frac{a_q}{4} \sqrt{\left(\frac{\pi}{\alpha}\right)^3} J_q(\phi_0) e^{-i\left(\frac{a_q^2}{8} - \frac{q\pi}{4}\right)} \\
& \left(J_{\frac{1}{2}}\left(\frac{a_q^2}{8}\right) + i J_{-\frac{1}{2}}\left(\frac{a_q^2}{8}\right) \right) \\
& + e^{-ik\sin(\theta)a} \sum_{q=-\infty}^{\infty} \frac{b_q}{4} \sqrt{\left(\frac{\pi}{\alpha}\right)^3} J_q(\phi_0) e^{-i\left(\frac{b_q^2}{8} - \frac{q\pi}{4}\right)} \\
& \left(J_{\frac{1}{2}}\left(\frac{b_q^2}{8}\right) + i J_{-\frac{1}{2}}\left(\frac{b_q^2}{8}\right) \right) \Bigg]
\end{aligned}
\tag{2.9}
$$

which as expected is the sum of two sets of infinite orders of plane wave. If we now use the fact that we are only interested in the +1 order of the upper input beam and the -1 order of the lower input beam to destructively interfere we can select the terms form the sums and find a_{min} so that the sum of the intensities is equal to zero,

$$
\begin{aligned}
U(0,0,z) = U_0 h_0 \sqrt{\left(\frac{\pi}{\alpha}\right)^3} \Bigg[& e^{ik\sin(\theta)a} \left(\frac{a_{-1}}{4} J_{-1}(\phi_0) e^{-i\left(\frac{a_{-1}^2}{8\alpha} - \frac{-\pi}{4}\right)} \right. \\
& \left. \left(J_{\frac{1}{2}}\left(\frac{a_{-1}^2}{8\alpha}\right) + i J_{-\frac{1}{2}}\left(\frac{a_{-1}^2}{8\alpha}\right) \right) \right) \\
& + e^{-ik\sin(\theta)a} \left(\frac{b_1}{4} J_1(\phi_0) e^{-i\left(\frac{b_1^2}{8\alpha} - \frac{\pi}{4}\right)} \right. \\
& \left. \left(J_{\frac{1}{2}}\left(\frac{b_1^2}{8\alpha}\right) + i J_{-\frac{1}{2}}\left(\frac{b_1^2}{8\alpha}\right) \right) \right) \Bigg] \overset{!}{=} 0.
\end{aligned}
\tag{2.10}
$$

We find that in order to archive destructive interference, the grating needs to be moved by

$$
a_{min} = \frac{\Lambda}{2}\left(\frac{3}{4} + n\right), \quad n \in \mathbb{Z}.
\tag{2.11}
$$

2.2 Achromatic nulling

When the setup is configured for a specific wavelength, the incident angle for that wavelength is determined by the grating equation, combined with the requirement that the ±1 diffraction orders must exit the grating at an angle of 0°. If light of a
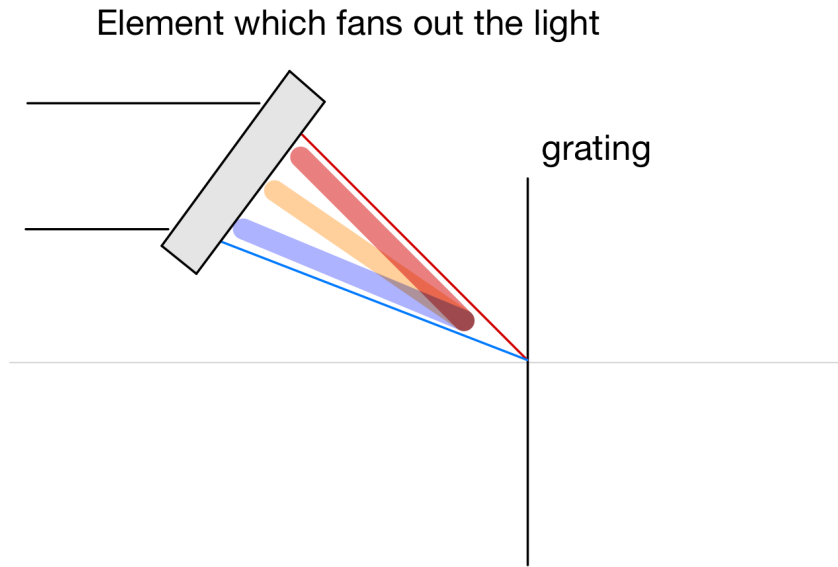
Element which fans out the light

grating

Figure 2.3: Illustration of a possible implementation to achieve achromatic nulling by using a diffractive optical element that "fans out" incoming light based on its wavelength. This ensures that each wavelength enters the grating at the optimal incident angle for nulling.

different wavelength is introduced at the same incident angle, the $\pm$ first orders will not exit at 0°. However, by adjusting the incident angle for the new wavelength, it is possible to achieve null across multiple wavelengths, thereby broadening the range of the null effect. This however does not mean, that the throughput is also constant over a range of wavelengths. This could for example be implemented by adding a material with a diffractive property to "fan" out the light based on its wavelengths, so that each light beam has the needed incoming angle to achieve nulling. An illustration of such an element can be seen in figure 2.3.

Chapter 3

Proposed experimental setup and expected performance

In the following chapter we propose an experimental setup visualized in Figure 3.1. It consists of three elements. Firstly a laser which in this setup is a Helium Neon laser. Secondly, a Keplerian telescope will magnify the beam from its original diameter of 0.65 mm to a diameter of 48.5 mm. This magnification value is arbitrary and was chosen because only a limited set of lenses were available. Working in this order of size is also easier for alignment purposes. The magnified beam then hits a mask which consists of two holes of radius $r = 1.5mm$ which are separated by a distance of $38.68mm$. There, the two monochromatic beams which later hit the grating are created. Thirdly the main part of the experiment, where the two beams are focused on the grating and split into the different orders and interfere. Here, it is important to note that the grating, which is positioned between the two lenses on the right side of figure 3.1 is placed on a piezo stage so that it can be precisely moved in the regime of $10^{-6}m$. Table 3.1 provides an overview of the lenses needed in this setup.

The optical elements used in this setup were chosen based on a balance between compatibility, modularity, and optical performance. All selected components are sourced from Thorlabs, as they are compatible with their cage system, which provides a highly modular framework for experimental setups. This modularity allows precise alignment, allows for easier modifications in future modifications, and enables the setup to be disassembled and reassembled with minimal realignment effort.

The beam expansion system was designed to achieve the necessary beam diameter before entering the diffraction section. The selection of lenses involved a trade-off between focal length and diameter, as only a limited number of read-
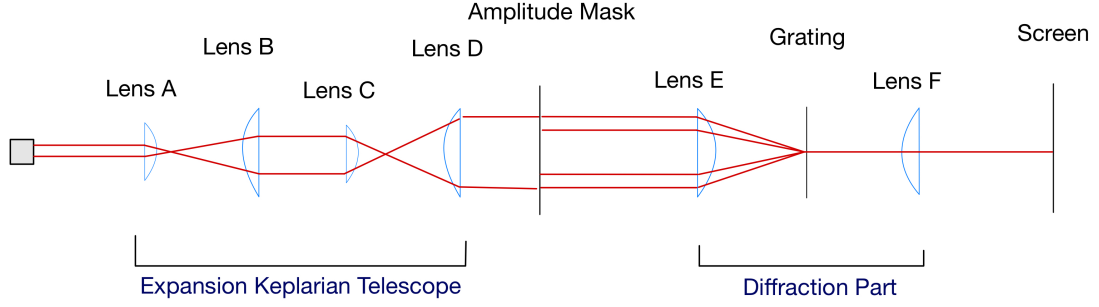
Figure 3.1: Schematic of the optical setup for the grating nuller experiment. The system consists of two main sections: an Expansion Keplerian Telescope and a Diffraction Part. The Keplerian telescope (Lenses A, B, and C) expands the beam before it passes through a amplitude mask. The beam is then collimated and directed towards the diffraction section, where it interacts with the grating (after passing through lenses D and E). Finally, lens F focuses the diffracted beam onto a screen for analysis.

Table 3.1: List of optical elements used in the experimental setup. Lens labels (A-F) correspond to those in Figure 3.1.

Component Group	Element (Label)	Specification
First Beam Expander	AC080-016-A (Lens A)	$f = 16$ mm, Diameter: 8 mm, ARC: 400-700 nm
	AC254-400-A (Lens B)	$f = 400$ mm, Diameter: 25.4 mm, ARC: 400-700 nm
Second Beam Expander	AC254-050-A (Lens C)	$f = 50$ mm, Diameter: 25.4 mm, ARC: 400-700 nm
	AC508-150-A (Lens D)	$f = 150$ mm, Diameter: 50.8 mm, ARC: 400-700 nm
Diffraction Section	AC508-100-A (Lens E)	$f = 100$ mm, Diameter: 50.8 mm, ARC: 400-700 nm
	GT13-03 (Grating)	Ruled Diffraction Grating, 300 lines/mm
	AC508-100-A (Lens F)	$f = 100$ mm, Diameter: 50.8 mm, ARC: 400-700 nm

ily available lenses were suitable for the setup. A compromise was made between achieving sufficient magnification and ensuring that the expanded beam does not exceed the aperture of the following lens. At the same time, the beam needed to be large enough to pass through the phase mask without excessive difficulty in handling alignment, while still maintaining a size suitable for effective diffraction at the grating.

The chosen grating is a GT13-03 ruled diffraction grating, with a line density of 300 lines/mm, corresponding to a grating period of:

$$\Lambda = \frac{1 \times 10^{-3} m}{300} = 3.33\,\mu\text{m}. \tag{3.1}$$

It is important to note that sinusoidal gratings were not readily available for the given wavelength range, leaving the blazed grating as the only available option. This introduces a challenge for later measurements, as the grating is not axis symmetric, which disrupts the symmetry of the optical setup. Therefore, the intensity of the upper and lower beams are not identical, affecting the nulling condition. One possible solution is to modify the intensity of one of the diffraction orders, ensuring that the outgoing intensities of both beams are equal, thereby allowing a proper null to be achieved.

The incident angle θ_{in} is selected to ensure that the first diffraction orders satisfy the nulling condition of leaving the grating at an angle of 0.

Given a central wavelength of $\lambda = 633$ nm and first-order diffraction ($m = \pm 1$), the calculated incident angle for both beams is 0.193 rad.

3.1   Performance simulations

To visualize the theoretical analysis of the grating nuller, an analytical study in Python was conducted to verify the conditions for nulling and to understand the systems behavior under different configurations. The analysis models the interference of two beams with a total input intensity of

$$I_{\text{input, total}} = I_1 + I_2 = 1 + 1 = 2,$$

which pass through a sinusoidal phase grating. The phase grating is an optical element with a periodically varying refractive index or thickness that changes the phase of an incoming wavefront without significantly affecting its amplitude. Unlike amplitude gratings, which partially block or absorb light, phase gratings alter the

optical path length, leading to diffraction into multiple orders. A sinusoidal grating was chosen because its symmetry provides an upper estimate for evaluating the theoretical throughput for a blazed grating, as used in the proposed setup. The key parameters include:

- **Wavelength** (λ): 633 nm (He-Ne laser).

- **Grating period** (Λ): 3.3×10^{-6} m.

- **Propagation distance** (z): 0.1 m.

- **Diffraction orders** (q_a, q_b): Used to compute interference patterns for different grating positions.

- **Incoming intensity** (U_0): Intensity of the incoming beams.

As our goal is trying to understand the theoretical limitations of the proposed setup we chose to look at the HeNe laser wavelength of 633nm. The electric fields of the ±1 orders of the beams (U_A and U_B) after passing through the grating were calculated by determining the electric field at position $x = y = 0$ using Fourier optics formalism. The total intensity was then computed as the square of the electric field as derived in Appendix 6.1:

$$I_{\text{total}} \propto \left| U_0 h_0 \sqrt{\left(\frac{\pi}{\alpha}\right)^3} \frac{a_{-1}}{4} J_1(\phi_0) \left(J_{\frac{1}{2}}\left(\frac{a_{-1}}{8\alpha}\right) + i J_{-\frac{1}{2}}\left(\frac{a_{-1}}{8\alpha}\right) \right) e^{\frac{b_{-1}^2}{8\alpha}} 2 \cos\left(k \sin(\theta) a - \frac{\pi}{4} \right) \right|^2$$

The results of the analysis are presented in figure 3.2. This plot illustrates the intensity as a function of the displacement a, showing the sum of the $+1$ and -1 diffraction orders. Periodic zeros in the intensity can be observed, confirming the nulling conditions. The periodicity aligns with the theoretical displacement values as calculated in equation 2.11.

3.1.1 Nulling Conditions

The analysis derives a theoretical displacement values ($a_{\min}$) at which destructive interference occurs. For example, at $a = \Lambda/2 \times (3/4 + n)$, the intensity reached periodic zeros, indicating successful nulling.
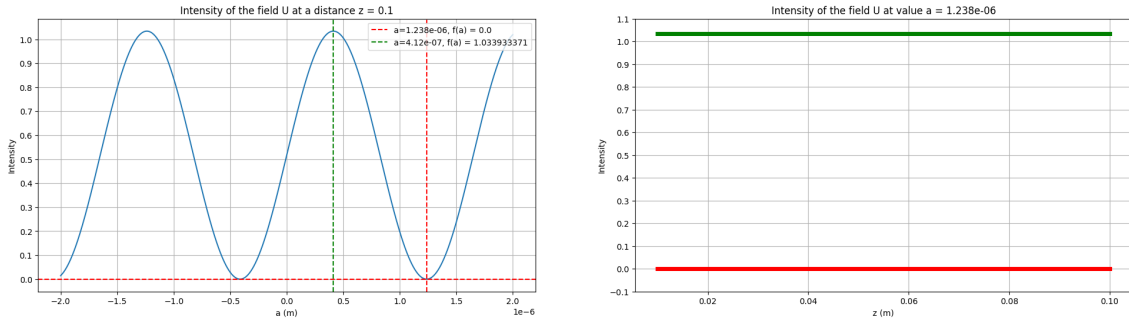
Figure 3.2: The left plot shows the intensity of the field U as a function of the parameter a at a fixed distance z = 0.1 m. The red dashed line marks $a = 1.238 \times 10^{-6}$ m, where the intensity is zero, while the green dashed line indicates $a = 4.12 \times 10^{-7}m$, where the intensity reaches a maximum of approximately 1.03. The right plot depicts the intensity of the field as a function of z for these two values of a . The red line corresponds to $a = 1.238 \times 10^{-6}m$, showing zero intensity across all z , while the green line represents 1.05, maintaining a high intensity throughout.
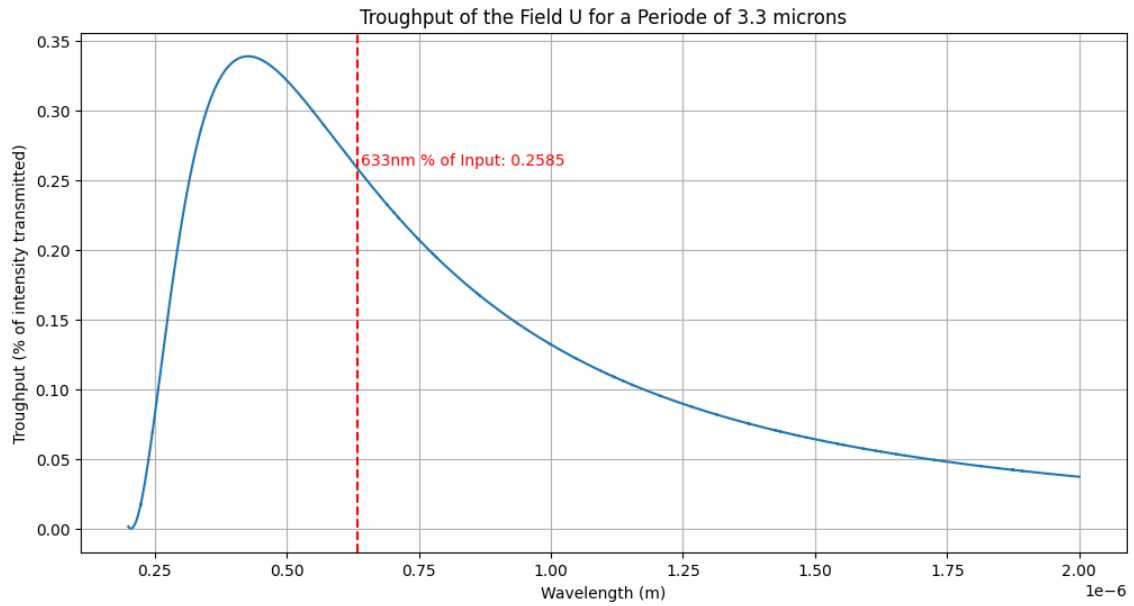

Figure 3.3: Throughput of the field U as a function of wavelength for a grating with a period of 3.3 microns. The plot shows the percentage of intensity transmitted for a single beam incident on the grating. The red dashed line marks the wavelength of 633 nm, corresponding to the HeNe laser used in our setup, with the throughput value indicated. The peak throughput occurs at a shorter wavelength before gradually decreasing as the wavelength increases.

3.1.2   Varying throughput with wavelength

To assess the feasibility of using a grating nuller, we analyze the expected through-put, which is directly related to the transmitted intensity. This is computed as the squared amplitude of the electric field, given by:

$$
U(0,0,z) = U_0 h_0 \sqrt{\left(\frac{\pi}{\alpha}\right)^3} e^{ik\sin(\theta)a} \left(\frac{a_{-1}}{4} J_{-1}(\phi_0) e^{-i\left(\frac{a_{-1}^2}{8\alpha} - \frac{-\pi}{4}\right)} \quad \left(J_{\frac{1}{2}}\left(\frac{a_{-1}^2}{8\alpha}\right) + i J_{-\frac{1}{2}}\left(\frac{a_{-1}^2}{8\alpha}\right)\right)\right),
$$
(3.2)

which describes the contribution of a single diffracted order. In this analysis, we focus on the first diffraction order for a single beam interacting with the grating. Due to the symmetry of the setup the first order of the second beam follows the exact same path.

From Fig. 3.3, we observe that the throughput varies with wavelength. The peak transmission occurs at wavelengths of about 450nm with a 34% throughput before decreasing monotonically for longer wavelengths. For the He-Ne laser wavelength ($\lambda = 633nm$), which corresponds to our proposed experimental setup, we find that under ideal conditions with a sinusoidal grating, approximately 25% of the incident intensity is expected to be transmitted through the grating. This aligns with theoretical expectations for sinusoidal diffraction gratings, where the energy is distributed across multiple diffraction orders.

Chapter 4

Discussion

The promise of a grating nuller in nulling interferometry lies in its intrinsic achromaticity, enabling effective nulling over a broad wavelength range. By utilizing a phase grating, the system achieves nulling with an elegant and minimalistic setup, in contrast to more complex interferometric designs like those employed in the NICE setup.

Another promising feature is the geometric simplicity of the grating nuller. While its symmetric configuration along the propagation axis provides a structured and well-defined setup, its impact on alignment requirements remains uncertain, as no detailed analysis of alignment tolerances or stability has been conducted. However, the symmetry may contribute to reducing systematic errors introduced by misalignment, which could be advantageous for space-based applications where in-flight adjustments are challenging.

The primary challenge associated with the grating nuller is its expected throughput. As discussed in Chapter 3, a sinusoidal phase grating theoretically yields a throughput of approximately 34%. However, real-world performance is likely to be lower due to various potential error sources, such as alignment imperfections and fabrication inconsistencies.

The main concern regarding the setup is the use of available off-the-shelf components, particularly blazed gratings. Unlike a sinusoidal phase grating, a blazed grating disrupts the intrinsic symmetry of the setup, which is a fundamental aspect of its functionality. This asymmetry introduces imbalances in beam intensities, affecting the nulling efficiency and the throughput. To accurately measure both the null depth and throughput, additional optical elements would be required to compensate for the intensity imbalance introduced by the blazed grating, further

limiting the expected throughput. Specifically, elements would need to be incorporated to dim the beam favored by the grating, ensuring it aligns with the intensity of the second beam.

Most importantly, the question remains whether the intensity of a phase grating could ever possibly exceed 50%. This question arises from the observation that an intensity plot of a grating presents a symmetric pattern, indicating that the +1 and -1 orders have the same intensity when the grating is axis-symmetric. Consequently, even if we employ a grating that somehow directs all its intensity into the first order, we can achieve a maximum intensity of 50%. Therefore, it remains uncertain whether a grating nuller can genuinely be a useful tool in praxis. A further theoretical model of such a nuller is essential as a first step, providing the foundation for experimental verification.

Chapter 5

Conclusion and Outlook

This report explored the potential of using a grating nuller in interferometry, particularly in the context of potentially using these methods in the LIFE mission. The grating nuller operates by diffracting incoming starlight to create destructive interference, effectively suppressing stellar light while allowing faint exoplanet signals to pass through. Its inherent achromaticity makes it an attractive candidate for an simplified nulling setup.

To evaluate the performance of the grating nuller, we derived analytical expressions for the null position and throughput of the grating, establishing a theoretical description using Fourier Optics. Under ideal conditions, a sinusoidal phase grating theoretically is expected to achieves a throughput of 34%, with a possible fundamental symmetry constraint preventing throughput from exceeding 50%. A simplified optical setup was designed to test the concept, and simulations suggest that the grating effectively nulls light across a broad wavelength range.

However, given these limitations, the practical feasibility of a grating nuller as a standalone solution for missions like LIFE remains unlikely. The necessary validation in the optical range is still lacking. Future research should test the limitations of such a grating nuller, particularly regarding throughput in the simpler optical range, to provide an indication of its practical usefulness.

Chapter 6

Appendix

6.1 Full derivation of the Intensity at x=y=0, at distance z using Fourier Optics

In this section, we provide the detailed calculations for the field after the grating. We start by considering the modified field at $z = 0$:

$$U'(x, y, z = 0) = t(x')U(x, y, z = 0)$$

$$= \sum_{q=-\infty}^{\infty} J_q(\phi_0)e^{i\frac{2\pi qx}{\Lambda}}(U_A(x+a) + U_B(x+a)) \tag{1}$$

$$= U_0 \left(e^{ik\sin(\theta)a} \sum_{q=-\infty}^{\infty} J_q(\phi_0)e^{i\left(\frac{2\pi qx}{\Lambda}+k\sin(\theta)\right)x} \right. \tag{2}$$

$$\left. + e^{-ik\sin(\theta)a} \sum_{q=-\infty}^{\infty} J_q(\phi_0)e^{i\left(\frac{2\pi qx}{\Lambda}-k\sin(\theta)\right)x} \right)$$

$$= U_0 \left(e^{-ik\sin(\theta)a} \sum_{q=-\infty}^{\infty} J_q(\phi_0)e^{ia_qx} + e^{ik\sin(\theta)a} \sum_{q=-\infty}^{\infty} J_q(\phi_0)e^{ib_qx} \right) \tag{3}$$

Here we used the Jacobi-Anger expansion [13] given by:

$$e^{iz\sin\theta} \equiv \sum_{n=-\infty}^{\infty} J_n(z)e^{in\theta}$$

where $J_n(z)$ are the Bessel functions of the first kind, z is the argument of the Bessel function, and θ is the angle, to go from (2) to (3). We also defined $a_q = \frac{2\pi qx}{\Lambda} + k\sin(\theta)$

and $b_q = \frac{2\pi qx}{\Lambda} - k\sin(\theta)$ for convenience.

The field at a distance $z = d$ is then given by the integral in Eq. 2.8. We are only interested in the value at $x = 0, y = 0$, thus we can write the final expression for the field at $x = 0, y = 0, z = d$ as:

$$U(0,0,z) = \frac{e^{ikz}}{i\lambda z} \iint_{-\infty}^{\infty} U_0 \left(e^{-ik\sin(\theta)a} \sum_{q=-\infty}^{\infty} J_q(\phi_0)e^{ia_q x'} \right.$$
$$\left. + e^{ik\sin(\theta)a} \sum_{q=-\infty}^{\infty} J_q(\phi_0)e^{ib_q x'} \right) e^{\frac{ik}{2z}(x'^2+y'^2)} dx'dy' \tag{1}$$

$$= U_0 h_0 \int_0^{\infty} \int_0^{2\pi} \left(e^{-ik\sin(\theta)a} \sum_{q=-\infty}^{\infty} J_q(\phi_0)e^{ia_q r' \cos(\phi')} \right.$$
$$\left. + e^{ik\sin(\theta)a} \sum_{q=-\infty}^{\infty} J_q(\phi_0)e^{ib_q r' \cos(\phi')} \right) e^{i\alpha r'^2} r' dr' d\phi' \tag{2}$$

We used cylindrical coordinates to simplify the calculations. We now only observe the q-th term from the first sum. Well see that the other term follows identically.

$$\int_0^{\infty} \int_0^{2\pi} J_q(\phi_0)e^{ia_q r' \cos(\phi')} e^{i\alpha r'^2} d\phi' \, dr' \tag{1}$$

$$= \int_0^{\infty} \int_0^{2\pi} J_q(\phi_0) \sum_{m=-\infty}^{\infty} i^m J_m(a_q r')e^{im\phi'} e^{i\alpha r'^2} r' \, d\phi' \, dr' \tag{2}$$

$$= 2\pi J_q(\phi_0) \int_0^{\infty} \sum_{m=-\infty}^{\infty} i^m J_m(a_q r')\delta(m)e^{i\alpha r'^2} r' \, dr' \tag{3}$$

$$= 2\pi J_q(\phi_0) \int_0^{\infty} J_0(a_q r')e^{i\alpha r'^2} r' \, dr' \tag{4}$$

$$= \frac{a_q}{4} \sqrt{\left(\frac{\pi}{\alpha}\right)^3} J_q(\phi_0)e^{-i\left(\frac{a_q^2}{8} - \frac{q\pi}{4}\right)} \left(J_{\frac{1}{2}}\left(\frac{a_q^2}{8}\right) + iJ_{-\frac{1}{2}}\left(\frac{a_q^2}{8}\right) \right) \tag{5}$$

Here, we use the following identities and steps:

1. **Jacobi-Anger Expansion:** The transition from (1) to (2) is obtained by applying the Jacobi-Anger identity for the cosine term:

$$e^{ia_q r' \cos(\phi')} = \sum_{m=-\infty}^{\infty} i^m J_m(a_q r')e^{im\phi'}.$$

2. **Integral of Exponentials:** The transition from (2) to (3) utilizes the fact that the integral of an exponential function over a full period of $e^{im\phi'}$ is a Dirac delta function:

$$\int_0^{2\pi} e^{im\phi'} d\phi' = 2\pi\delta(m).$$

This effectively selects the $m = 0$ term.

3. **Zero for Non-zero m':** In step (3), we use the property that $\delta(m)$ ensures only the term with $m = 0$ contributes. Hence, we are left with the Bessel function $J_0(a_q r')$ in the integrand.

4. **Integral Identity:** The final step (4) to (5) utilizes the following integral identity for Bessel functions [14][15]:

$$\int_0^\infty J_v(b\rho)e^{i\alpha\rho^2}\rho\, d\rho = \frac{b}{8}\left(\frac{\sqrt{\pi}}{\alpha^{3/2}}\right)e^{-i\left(\frac{b^2}{8\alpha} - \frac{v\pi}{4}\right)}\left[J_{\frac{v+1}{2}}\left(\frac{b^2}{8\alpha}\right) + iJ_{\frac{v-1}{2}}\left(\frac{b^2}{8\alpha}\right)\right],$$

which gives the final result in (5).

If we put this together for the full integral we get:

$$
\begin{aligned}
U(0,0,z) = U_0 h_0 \Bigg[& e^{ik\sin(\theta)a} \sum_{q=-\infty}^{\infty} \frac{a_q}{4}\sqrt{\left(\frac{\pi}{\alpha}\right)^3} J_q(\phi_0) e^{-i\left(\frac{a_q^2}{8} - \frac{q\pi}{4}\right)} \\
& \left(J_{\frac{1}{2}}\left(\frac{a_q^2}{8}\right) + iJ_{-\frac{1}{2}}\left(\frac{a_q^2}{8}\right)\right) \\
& + e^{-ik\sin(\theta)a} \sum_{q=-\infty}^{\infty} \frac{b_q}{4}\sqrt{\left(\frac{\pi}{\alpha}\right)^3} J_q(\phi_0) e^{-i\left(\frac{b_q^2}{8} - \frac{q\pi}{4}\right)} \\
& \left(J_{\frac{1}{2}}\left(\frac{b_q^2}{8}\right) + iJ_{-\frac{1}{2}}\left(\frac{b_q^2}{8}\right)\right) \Bigg]
\end{aligned}
\tag{6.1}
$$

If we now observe the -1 order of the U_A and the +1 order of U_B we find that

$$U(0,0,z) = U_0 h_0 \sqrt{\left(\frac{\pi}{\alpha}\right)^3} \left[e^{ik\sin(\theta)a} \left(\frac{a_{-1}}{4} J_{-1}(\phi_0) e^{-i\left(\frac{a_{-1}^2}{8\alpha} - \frac{-\pi}{4}\right)} \right. \right.$$

$$\left. \left(J_{\frac{1}{2}}\left(\frac{a_{-1}^2}{8\alpha}\right) + i J_{-\frac{1}{2}}\left(\frac{a_{-1}^2}{8\alpha}\right) \right) \right)$$

$$+ e^{-ik\sin(\theta)a} \left(\frac{b_1}{4} J_1(\phi_0) e^{-i\left(\frac{b_1^2}{8\alpha} - \frac{\pi}{4}\right)} \right.$$

$$\left. \left. \left(J_{\frac{1}{2}}\left(\frac{b_1^2}{8\alpha}\right) + i J_{-\frac{1}{2}}\left(\frac{b_1^2}{8\alpha}\right) \right) \right) \right] \overset{!}{=} 0$$

(6.2)

As $a_{-1} = \frac{-2\pi}{\Lambda} + k\sin(\theta) = -b_1$, it follows that $a_{-1}^2 = b_1^2$, and because $J_{-1}(x) = -J_1(x)$, the expression simplifies to:

$$U_0 h_0 \sqrt{\left(\frac{\pi}{\alpha}\right)^3} \frac{a_{-1}}{4} J_1(\phi_0) \left(J_{\frac{1}{2}}\left(\frac{a_{-1}}{8\alpha}\right) + i J_{-\frac{1}{2}}\left(\frac{a_{-1}}{8\alpha}\right) \right) e^{\frac{b_{-1}^2}{8\alpha}} 2\cos\left(k\sin(\theta)a - \frac{\pi}{4} \right).$$

To find the zeros, we solve:

$$\cos\left(k\sin(\theta)a - \frac{\pi}{4} \right) = 0.$$

The solutions are given by

$$a = \pi \frac{\frac{3}{4} + n}{k\sin(\theta)} = \frac{\Lambda}{2}\left(\frac{3}{4} + n \right), \quad n \in \mathbb{Z}.$$

Here we used the definition of k and that due to the design of the experiment

$$\sin(\theta) = \frac{\lambda}{\Lambda}$$

where Λ is the grating constant.

Bibliography

[1] NASA. Exoplanet Catalog. https://science.nasa.gov/exoplanets/exoplanet-catalog/, 2024. Accessed: 2024-11-20.

[2] Sascha P. Quanz, Jens Kammerer, Denis Defrère, Olivier Absil, Adrian M. Glauser, and Daniel Kitzmann. Exoplanet science with a space-based mid-infrared nulling interferometer, 2018. URL https://arxiv.org/abs/1807.06088.

[3] Sascha Patrick Quanz. LIFE-The Large Interferometer for Exoplanets. https://video.ethz.ch/lectures/d-phys/2024/autumn/402-0368-07L.html, 2024. Lecture in Lecture Series "Space Research and Exploration", ETH Zurich. Accessed: 2024-11-21.

[4] Sascha P. Quanz, Olivier Absil, Willy Benz, Xavier Bonfils, Jean-Philippe Berger, Denis Defrère, Ewine van Dishoeck, David Ehrenreich, Jonathan Fortney, Adrian Glauser, John Lee Grenfell, Markus Janson, Stefan Kraus, Oliver Krause, Lucas Labadie, Sylvestre Lacour, Michael Line, Hendrik Linz, Jérôme Loicq, Yamila Miguel, Enric Pallé, Didier Queloz, Heike Rauer, Ignasi Ribas, Sarah Rugheimer, Franck Selsis, Ignas Snellen, Alessandro Sozzetti, Karl R. Stapelfeldt, Stephane Udry, and Mark Wyatt. Atmospheric characterization of terrestrial exoplanets in the mid-infrared: biosignatures, habitability, and diversity. *Experimental Astronomy*, 54(2–3):1197–1221, September 2021. ISSN 1572-9508. doi: 10.1007/s10686-021-09791-z. URL http://dx.doi.org/10.1007/s10686-021-09791-z.

[5] Daniel Rouan. Nulling Interferometry. In Muriel Gargaud, Ricardo Amils, José Cernicharo Quintanilla, Henderson James (Jim) Cleaves, William M. Irvine, Daniele L. Pinti, and Michel Viso, editors, *Encyclopedia of Astrobiology*, pages 1152–1155. Springer Berlin Heidelberg, Berlin, Heidelberg, 2011. ISBN 978-3-642-11274-4. doi: 10.1007/978-3-642-11274-4_1088. URL https://doi.org/10.1007/978-3-642-11274-4_1088.

[6] T. Velusamy, R. Angel, A. Eatchel, D. Tenerelli, and N. Woolf. Single and double Bracewell nulling interferometer in space. *Astronomy and Astrophysics*, 539:631–636, 09 2003.

[7] Colin Dandumont, Denis Defrère, Jens Kammerer, Olivier Absil, Sascha P. Quanz, and Jérôme Loicq. Exoplanet detection yield of a space-based Bracewell interferometer from small to medium satellites. *Journal of Astronomical Telescopes, Instruments, and Systems*, 6:035004, July 2020. doi: 10.1117/1.JATIS.6.3.035004.

[8] R. N. Bracewell. Detecting nonsolar planets by spinning infrared interferometer. *Nature*, 274:780–781, 1978. doi: 10.1038/274780a0.

[9] Felix A. Dannert, Maurice Ottiger, Sascha P. Quanz, Romain Laugier, Emile Fontanet, Adrian Gheorghe, Olivier Absil, Colin Dandumont, Denis Defrere, Carlos Gascon, Adrian M. Glauser, Jens Kammerer, Tim Lichtenberg, Hendrik Linz, and Jérôme Loicq. Large Interferometer For Exoplanets (LIFE): II. Signal simulation, signal extraction, and fundamental exoplanet parameters from single-epoch observations. *Astronomy & Astrophysics*, 664:A22, August 2022. ISSN 1432-0746. doi: 10.1051/0004-6361/202141958. URL `http://dx.doi.org/10.1051/0004-6361/202141958`.

[10] LIFE Team. Learn About LIFE. `https://life-space-mission.com/learn/`, 2024. Accessed: 2024-11-21.

[11] Stefan Martin, Gene Serabyn, Kurt Liewer, and Bertrand Mennesson. Achromatic broadband nulling using a phase grating. *Optica*, 4(1):110–113, Jan 2017. doi: 10.1364/OPTICA.4.000110. URL `https://opg.optica.org/optica/abstract.cfm?URI=optica-4-1-110`.

[12] Joseph W. Goodman. *Introduction to Fourier Optics*. McGraw-Hill, New York, 2nd edition, 1996. ISBN 978-0070242548.

[13] George B. Arfken and Hans J. Weber. *Mathematical Methods for Physicists*. Elsevier, Amsterdam, 7th edition, 2012. ISBN 978-0-12-384654-9. Jacobi-Anger expansion is discussed on page 687. Available online at `https://physicaeducator.wordpress.com/wp-content/uploads/2018/02/mathematical-method-for-physicist-by-arfken-and-weber.pdf`.

[14] Saifollah Rasouli and Ali Mohammad Khazaei. An azimuthally-modified linear phase grating: Generation of varied radial carpet beams over different diffraction orders with controlled intensity sharing among the generated beams. *Scientific Reports*, 9(1):1–10, 2019. doi: https://doi.org/10.1038/s41598-019-48757-2. URL `https://doi.org/10.1038/s41598-019-48757-2`.

[15] Daniel Zwillinger, Victor Moll, I.S. Gradshteyn, and I.M. Ryzhik, editors. *Table of Integrals, Series, and Products (Eighth Edition)*. Academic Press, Boston, eighth edition edition, 2014. ISBN 978-0-12-384933-5. doi: https://doi.org/10.1016/C2010-0-64839-5. URL `https://doi.org/10.1016/C2010-0-64839-5`.

Use of Generative Artificial Intelligence

In accordance with ETH Zurich's guidelines on academic integrity and the responsible use of artificial intelligence[1], and with permission of my supervisor I acknowledge that generative AI tools like ChatGPT and Copilot, were used in the creation of this report. These tools were employed to assist in structuring and drafting content, refining formulations improving clarity and helping with code in Python an LaTeX. However, all conceptual work, calculations, analysis, and interpretations remain my own, and I take full responsibility for the content and accuracy of this

---

[1]`https://library.ethz.ch/en/researching-and-publishing/scientific-writing-at-eth-zurich/plagiat-und-kuenstliche-intelligenz-ki.html`

report. I have ensured that the use of AI tools adheres to the principles of academic integrity and does not replace independent intellectual contributions. Any AI-generated text has been critically reviewed and modified to meet the academic standards of ETH Zurich.

Title of work:

Analysis of a Grating Nuller for LIFE

Thesis type and date:

Semester Thesis, March, 2025

Supervision:

Prof. Dr. Sascha Patrick Quanz
Thomas Birbacher

Student:

Name:	Niklas Viebig
E-mail:	nviebig@student.ethz.ch
Legi-Nr.:	20-944-286

Statement regarding plagiarism:

By signing this statement, I affirm that I have read and signed the Declaration of Originality, independently produced this paper, and adhered to the general practice of source citation in this subject-area.

Declaration of Originality:

http://www.ethz.ch/faculty/exams/plagiarism/confirmation_en.pdf

Zurich, 28. 4. 2025: